NiYAl-Derived Nanoporous Catalysts for Dry Reforming of Methane

Syota Imada [1], Xiaobo Peng [2], Zexing Cai [1,3], Abdillah Sani Bin Mohd Najib [2], Masahiro Miyauchi [4], Hideki Abe [2] and Takeshi Fujita [1,*]

[1] School of Environmental Science and Engineering, Kochi University of Technology, 185 Miyanokuchi, Tosayamada, Kami City, Kochi 782-8502, Japan; 245105w@gs.kochi-tech.ac.jp (S.I.); cai.zexing@kochi-tech.ac.jp (Z.C.)
[2] National Institute for Materials Science, 1-1 Namiki, Tsukuba, Ibaraki 305-0044, Japan; peng.xiaobo@nims.go.jp (X.P.); abdillah.sani@nims.go.jp (A.S.B.M.N.); ABE.Hideki@nims.go.jp (H.A.)
[3] School of Physics and Electronic Engineering, Xinyang Normal University, Xinyang 464000, China
[4] Tokyo Institute of Technology, 2-12-1 Ookayama, Meguro-ku, Tokyo 152-8552, Japan; mmiyauchi@ceram.titech.ac.jp
[*] Correspondence: fujita.takeshi@kochi-tech.ac.jp

check for updates

Abstract: Dry reforming of methane can be used for suppressing the rapid growth of greenhouse gas emissions. However, its practical implementation generally requires high temperatures. In this study, we report an optimal catalyst for low-temperature dry reforming of methane with high carbon coking resistance synthesized from NiYAl alloy. A facile two-step process consisting of preferential oxidation and leaching was utilized to produce structurally robust nanoporous Ni metal and Y oxides from $NiYAl_4$. The catalyst exhibited an optimal carbon balance (0.96) close to the ideal value of 1.0, indicating the optimized dry reforming pathway. This work proposes a facile route of the structural control of active metal/oxide sites for realizing highly active catalysts with long-term durability.

Keywords: nanoporous catalyst; methane dry reforming; NiYAl alloy; preferential oxidation; long-term durability

1. Introduction

Continuously increasing greenhouse gas (CO_2) emissions trigger various climatic disasters and are gradually raising the sea level, which considerably decrease habitable areas. Therefore, developing a feasible method for the chemical or physical utilization of vast CO_2 quantities represents an urgent task. Methane (CH_4) is both a major component of natural gas and a greenhouse gas; hence, the dry reforming of methane (DRM, $CH_4 + CO_2 \rightarrow 2H_2 + 2CO$) could become a promising strategy for tackling excessive CO_2 output without disrupting the current infrastructure and converting it to valuable chemical products [1]. However, this reaction requires a relatively high temperature (>800 °C) because of its endothermicity ($\Delta H°_{298K} = 247$ kJ mol^{-1}), which results in significant heat degradation due to material sintering. When DRM is performed in a low-temperature range from 400 to 600 °C, corresponding to low-temperature DRM (LT-DRM), its side reactions become more thermodynamically dominant leading to significant carbon coking due to methane decomposition ($CH_4 \rightarrow 2H_2 + C(s)$) and the Boudouard reaction ($2CO \rightarrow CO_2 + C(s)$), that ultimately block the gas flow and cause a rupture of the reactor. Many heterogeneous (typically Ni-based) catalysts have been studied to date, and various modifications of the interactions between Ni atoms and oxide supports and/or structural design were considered [2–9]. To suppress a significant growth of carbon fabric on Ni particles, topological modification of the active sites located at the metal–oxide interface should be performed. Unlike the

conventional nanoparticle–oxide supports, a well-connected metal–oxide topology obtained from bulk alloy via preferential oxidation [10–12] or leaching (dealloying) [13,14] was found to be a critical structural design with a highly active metal–oxide interface and long-term stability.

Here, we report nanoporous catalysts derived from $NiYAl_x$ intermetallic precursors by combining preferential oxidation with leaching. As was shown in our previous study on binary NiY alloy [10], the preferential oxidation process resulted in the nanophase separation of Ni, Y oxide, and Al oxide in the precursor alloy, and the subsequent leaching process dissolved all Al components (Al and Al oxides) to yield a structurally robust nanoporous Ni/Y oxide catalyst. In the course of catalyst evaluation that involved intentional carbon accumulation, the obtained nanoporous catalyst was more resistant to carbon deposition than the conventional Ni-based (Ni/Al_2O_3) and Raney Ni catalysts for LT-DRM. In contrast to conventional chemical routes, the top-down process starting from bulk alloy can produce advanced materials with high catalytic activity and coking tolerance for methane conversion.

2. Materials and Methods

2.1. Preparation of Nanoporous Catalysts

The utilized catalyst fabrication route is outlined in Figure 1.
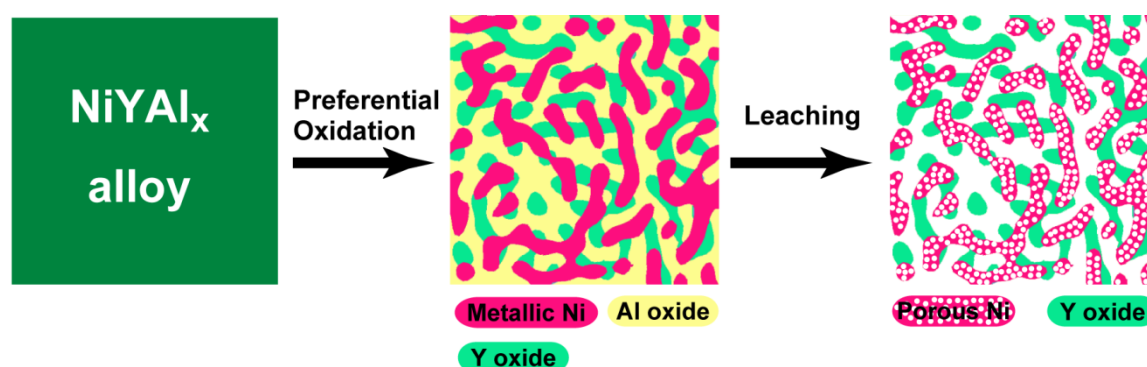
Figure 1. Schematic illustration of the catalyst preparation from $NiYAl_x$ alloys.

$Ni_{33.3}Y_{33.3}Al_{33.3}$, $Ni_{25}Y_{25}Al_{50}$, and $Ni_{16.7}Y_{16.7}Al_{66.6}$ (at.%) were selected as intermetallic precursors for NiYAl, $NiYAl_2$ and $NiYAl_4$, respectively, using the Ni–Al–Y ternary phase diagram [15]. Ingots were prepared by melting pure Ni, Y, and Al metals (>99.9 at.%) inside an Ar-protected arc melting furnace. The resulting Ni–Y–Al alloy ingots were ground in a mortar and sieved to obtain powder precursors with average particle sizes of 50–60 μm. During the preferential oxidation process, the Ni–Y–Al alloy precursors were heated in a gas stream consisting of CO (2 vol.%), O_2 (1 vol.%), and Ar (97 vol.%) at a flow rate of 60 mL min^{-1} and temperature of 873 K for 12 h to obtain phase-separated Ni–Y_2O_3–Al_2O_3 composites. To perform acid leaching, these composites (~0.5 g) were autoclaved in a 15 M NaOH solution at a pressure of 5 atm and temperature of 150 °C for 6 h to dissolve Al, followed by thorough rinsing with water and drying under air.

2.2. Preparation of Conventional Ni Catalysts

Ni/Al_2O_3 composite was prepared by a conventional impregnation method. Following the dissolution of $Ni(NO_3)_2 \cdot 6H_2O$ (0.8 g, Sigma-Aldrich, Louis, MO, USA) in ethanol (20 mL), Al_2O_3 powder (0.3 g, Sigma-Aldrich Louis, MO, USA) was added to the reaction solution. The resulting mixture was stirred for 8 h, after which ethanol was removed by evaporation at 353 K. Ni/Al_2O_3 catalyst was synthesized through the calcination of the obtained product in an H_2–Ar gas mixture (5 vol.% H_2) at 873 K for over 4 h.

To obtain Raney Ni catalyst, commercial Ni–Al (50/50 wt.%) precursor powder was purchased from Kojundo Chemical Laboratory CO., Ltd., Saitama, Japan. Approximately 0.5 g of this powder

was dealloyed in a 30 wt.% NaOH (97% Wako, Japan) solution for 4 h at 50 °C, rinsed thoroughly with water, and dried under air.

2.3. Microstructural Characterization

Microstructures of the obtained catalysts were characterized by scanning transmission electron microscopy (STEM, JEM-2100F, JEOL, Tokyo, Japan) and energy-dispersive x-ray spectroscopy (EDS, Ince Energy TEM 250, Oxford, Abingdon, UK). The analyzed samples were transferred onto a Cu grid without using a uniform carbon support film. X-ray diffraction (XRD) profiles were recorded using a Rigaku SmartLab X-ray diffractometer (Rigaku, Tokyo, Japan) with Cu Kα radiation (40 kV). Surface morphologies were observed by scanning electron microscope (SEM, Hitachi SU-8030, Tokyo, Japan) at an accelerating voltage of 15 kV. The deposited carbon present after the DRM process was evaluated using a thermal gravimetric-differential thermal analyzer (TG-DTA, NETZSCH, STA 2500, Selb, Germany) under air. The sharp mass loss above 500 °C corresponded to the combustion of carbon.

2.4. Catalytic Studies

LT-DRM was conducted inside a fixed-bed flow reactor with an inner diameter of 10 mm. A sample with a mass of 0.1 g was loaded into the reactor at 550 °C in a gas mixture of CH_4 (10 mL/min), CO_2 (10 mL/min), and N_2 (5 mL/min) with a total flow rate of 25 mL min^{-1} to accelerate the carbon accumulation process. The composition of the effluent gas was monitored by a gas chromatograph (Shimadzu, TCD, GC-8A) with a column made of activated charcoal. The formulas utilized for calculating consumption rates, formation rates, conversions, and the H_2/CO ratio are provided below [13]:

$$CH_4 \text{ conv. } [\%] = \frac{[CH_4]_{in} - [CH_4]_{out}}{[CH_4]_{in}} \times 100$$

$$CO_2 \text{ conv. } [\%] = \frac{[CO_2]_{in} - [CO_2]_{out}}{[CO_2]_{in}} \times 100$$

$$CH_4 \text{ consumption rate} = [CH_4]_{in} \text{ flow rate} \times CH_4 \text{ conv.}$$

$$CO_2 \text{ consumption rate} = [CO_2]_{in} \text{ flow rate} \times CO_2 \text{ conv.}$$

$$H_2 \text{ formation rate} = [CH_4]_{in} \text{ flow rate} \times \frac{[H_2]_{out}}{[CH_4]_{in}}$$

$$CO \text{ formation rate} = ([CH_4]_{in} \text{ flow rate} + [CO_2]_{in} \text{ flow rate}) \times \frac{[CO]_{out}}{[CH_4]_{in} + [CO_2]_{in}}$$

$$H_2/CO \text{ ratio} = \frac{H_2 \text{ formation ratio}}{CO \text{ formation ratio}}$$

where […]$_{in}$ and […]$_{out}$ represent the molar concentrations in the feed gas and effluent gas, respectively.

3. Results and Discussion

Intermetallic precursors were obtained by arc-melting, and the resulting $NiYAl_4$ (JCPDF#50-1236), $NiYAl_2$ (#76-8082), and NiYAl (#22-0008) compounds were identified in the as-made precursor alloys by XRD, as shown in Figure S1. The subsequent preferential oxidation via the CO + O_2 reaction induced the phase separation of Ni, Al_2O_3 (#04-0877), Y_2O_3 (#43-0661), and residual intermetallics according to Figure S2. After conducting high-pressure leaching to remove Al components, the resultant products were ultimately converted to Ni and $Y(OH)_3$ (Figure 2); the latter was subsequently converted to Y_2O_3 through a catalytic reaction in the next step. The conversion from $Y(OH)_3$ to Y_2O_3 was driven by the DRM reaction as well as heat treatment [13,16].
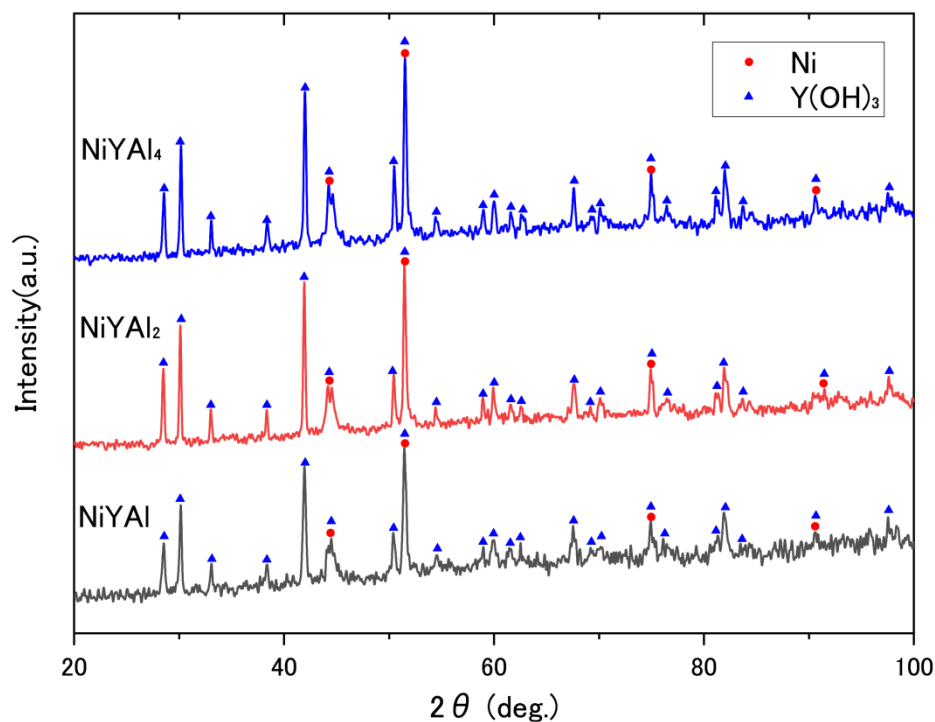
Figure 2. X-ray diffractograms of the nanoporous catalysts obtained from NiYAl$_4$, NiYAl$_2$, and NiYAl intermetallic precursors.

The obtained scanning electron microscope (SEM) images are displayed in Figure 3.
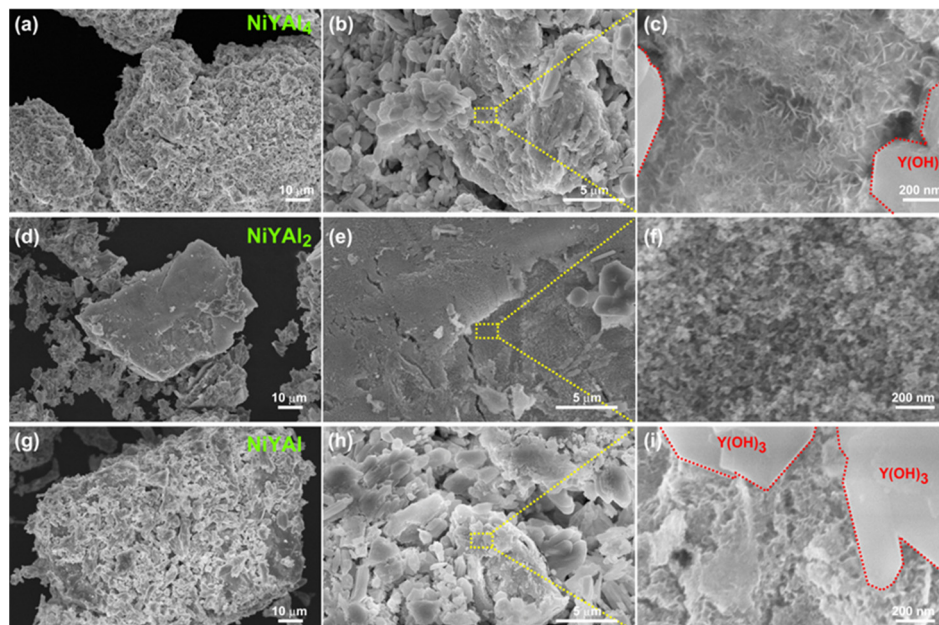
Figure 3. SEM images of the nanoporous catalysts derived from (**a**–**c**) NiYAl$_4$, (**d**–**f**) NiYAl$_2$, and (**g**–**i**) NiYAl intermetallic precursors.

The microstructures of the NiYAl- and NiYAl$_4$-derived samples contain mixed but distinct regions of squarish Y(OH)$_3$ and nanoporous Ni. The microstructure of the NiYAl$_2$-derived catalyst includes the nanoporous Ni and isolated Y(OH)$_3$ regions. The nanoporous Ni region in the NiYAl$_4$-based sample was analyzed by STEM–EDS, as shown in Figure 4.
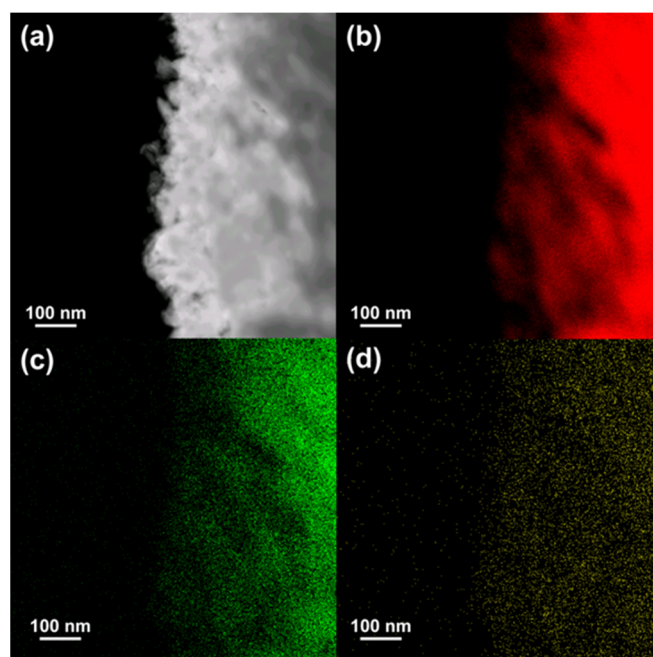
Figure 4. (**a**) STEM image and (**b**–**d**) energy-dispersive x-ray spectroscopy (EDS) chemical maps of the nanoporous Ni region in the NiYAl$_4$-derived sample showing the distributions of Ni (red), Y (green), and O (yellow) elements.

Its average pore size was approximately 30 nm, while the composition of the nanoporous Ni region in the sample, represented by the formula 91.9Ni–2.6Y–0.5Al–5O (at.%), was relatively uniform.

The catalytic properties of the nanoporous catalysts produced from NiYAl, NiYAl$_2$, and NiYAl$_4$ precursors are summarized in Table 1. Here, the conventional Ni/Al$_2$O$_3$ and Raney Ni catalysts serve as references. The H$_2$/CO ratio is an important indicator of the coking resistance (its ideal value is equal to one, while higher magnitudes of this parameter indicate a significant coking effect). Photographs of the initial and spent catalyst samples are shown in Figure S3. As expected from the increased volume in Figure S3, the spent NiYAl$_2$-derived sample demonstrated the most intense coking effect (H$_2$/CO ratio = 2.4), and the NiYAl$_4$-derived catalyst exhibited the weakest coking effect (H$_2$/CO ratio = 0.7). The XRD analysis (Figure 5a) reveals that the spent samples are composed of Ni and Y$_2$O$_3$ converted from Y(OH)$_3$. In addition, the carbon peaks with the highest intensity appear for the NiYAl$_2$-derived catalyst, whereas the smallest carbon peaks are observed for the NiYAl$_4$-derived one. The NiYAl$_4$-base sample exhibited no catalytic activity after the preferential oxidation (without etching), indicating that the final leaching process was an important step toward achieving the optimal catalyst microstructure. The conventional Ni/Al$_2$O$_3$ and Raney Ni catalysts also demonstrated strong coking effects (their H$_2$/CO ratios were 2.3 and 1.4, respectively). We calculated the carbon balance for these catalysts; carbon balance = {CO formation rate/(CH$_4$ consumption rate + CO$_2$ consumption rate)}, and the results are shown in Figure 5b. The conventional catalyst Ni/Al$_2$O$_3$ exhibits the lowest carbon balance of 0.31. Although Raney Ni shows a relatively higher carbon balance (0.74), the NiYAl$_4$-derived sample represented the optimal carbon balance (0.96) close to the ideal value of 1.0, indicating the optimal DRM pathway. The thermal gravimetric analysis (Figure S4) confirms that the spent NiYAl$_4$-derived sample exhibit the lowest amount of coking.

Table 1. Dry reforming of methane (DRM) parameters of various Ni catalysts including the nanoporous catalysts obtained from NiYAl, NiYAl$_2$, and NiYAl$_4$ intermetallic precursors in this study as well as conventional Ni/Al$_2$O$_3$ and Raney Ni catalysts. The NiYAl$_4$ sample showed no catalytic activity after the preferential oxidation (CO + O$_2$) without leaching.

Sample	CH$_4$ Conv. (%)	CO$_2$ Conv. (%)	CH$_4$ Consumption Rate (mmol h^{-1})	CO$_2$ Consumption Rate (mmol h^{-1})	H$_2$ Formation Rate (mmol h^{-1})	CO Formation Rate (mmol h^{-1})	H$_2$/CO Ratio
NiYAl$_4$	12	19	3.3	5.1	5.7	8.1	0.7
NiYAl$_2$	45	33	12	8.8	18	8.5	2.2
NiYAl	32	29	8.5	7.9	14	9.8	1.4
NiYAl$_4$ (CO + O$_2$)	0	0	-	-	-	-	-
Ni/Al$_2$O$_3$	56	37	15	10	18	7.7	2.3
Raney Ni	33	31	8.9	8.5	17	13	1.4

Reaction conditions: 0.1 g; 550 °C; CH$_4$ (10 mL/min), CO$_2$ (10mL/min), and N$_2$ (5 mL/min) with a total flow rate of 25 mL min^{-1}; 4–6 h.
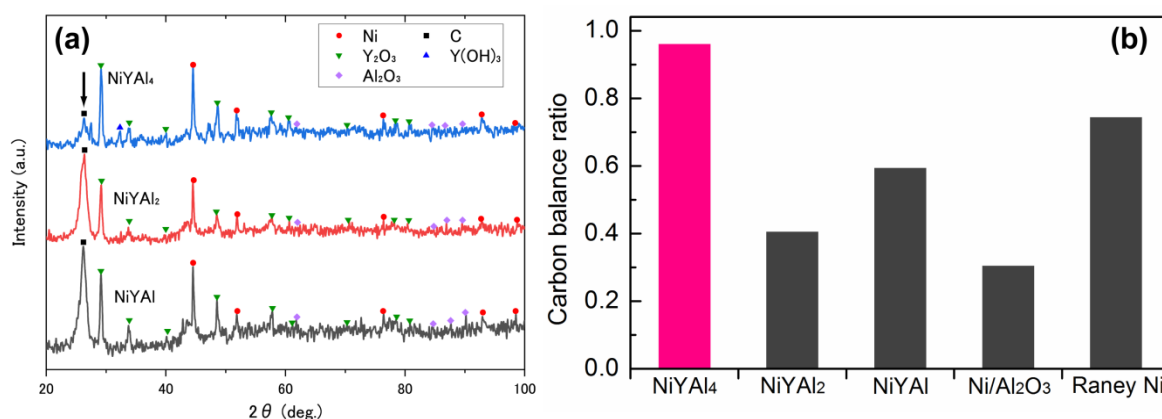
Figure 5. (**a**) X-ray diffractograms of the spent catalysts prepared from NiYAl$_4$, NiYAl$_2$, and NiYAl intermetallic precursors. The arrow indicates the position of the carbon peak. (**b**) Carbon balance ratio for the present catalysts and reference catalysts. Carbon balance = {CO formation rate/(CH$_4$ consumption rate + CO$_2$ consumption rate)}.

4. Conclusions

In this study, we fabricated nanoporous catalysts from NiYAl$_x$ intermetallic precursors by a combined process of preferential oxidation and leaching. The optimal catalyst obtained from NiYAl$_4$ possessed a structurally robust nanoporous Ni metal and Y oxide structure with high coking resistance for LT-DRM. The described facile fabrication process can be utilized for fabricating highly active catalysts with long-term stability from various binary, ternary, and quaternary metal alloys.

Author Contributions: S.I. fabricated the samples and conducted SEM/XRD characterizations. T.F. performed TEM characterization. X.P. and A.S.B.M.N. performed catalysis tests. T.F. and Z.C. wrote the manuscript. M.M., T.F., and H.A. supervised the entire research project. All authors have read and agreed to the published version of the manuscript.

Conflicts of Interest: The authors declare no conflict of interest.

References

1. Song, Y.; Ozdemir, E.; Ramesh, S.; Adishev, A.; Subramanian, S.; Harale, A.; Albuali, M.; Fadhel, B.A.; Jamal, A.; Moon, D.; et al. Dry reforming of methane by stable Ni-Mo nanocatalysts on single-crystalline MgO. *Science* **2020**, *367*, 777–781. [CrossRef] [PubMed]
2. Muraza, O.; Galadima, A. A review on coke management during dry reforming of methane. *Int. J. Energy Res.* **2015**, *39*, 1196–1216. [CrossRef]
3. Nair, M.M.; Kaliaguine, S. Structured catalysts for dry reforming of methane. *New J. Chem.* **2016**, *40*, 4049–4060. [CrossRef]
4. Lavoie, J.M. Review on dry reforming of methane, a potentially more environmentally-friendly approach to the increasing natural gas exploitation. *Front. Chem.* **2014**, *2*, 81. [CrossRef] [PubMed]
5. Kathiraser, Y.; Thisartarn, W.; Sutthiumporn, K.; Kawi, S. Inverse $NiAl_2O_4$ on $LaAlO_3-Al_2O_3$: Unique catalytic structure for stable CO_2 reforming of methane. *J. Phys. Chem. C* **2013**, *117*, 8120–8130. [CrossRef]
6. Ashok, J.; Bian, Z.; Wang, Z.; Kawi, S. Ni-phyllosilicate structure derived $Ni–SiO_2–MgO$ catalysts for bi-reforming applications: Acidity, basicity and thermal stability. *Catal. Sci. Technol.* **2018**, *8*, 1730–1742. [CrossRef]
7. Ni, J.; Chen, L.; Lin, J.; Kawi, S. Carbon deposition on borated alumina supported nano-sized Ni catalysts for dry reforming of CH_4. *Nano Energy* **2012**, *1*, 674–686. [CrossRef]
8. Bian, Z.; Suryawinata, I.Y.; Kawi, S. Highly carbon resistant multicore-shell catalyst derived from Ni-Mg phyllosilicate nanotubes@silica for dry reforming of methane. *Appl. Catal. B* **2016**, *195*, 1–8. [CrossRef]
9. Bian, Z.; Kawi, S. Sandwich-like Silica@Ni@Silica multicore–shell catalyst for the low-temperature dry reforming of methane: Confinement effect against carbon formation. *ChemCatChem* **2018**, *10*, 320–328. [CrossRef]
10. Shoji, S.; Peng, X.; Imai, T.; Kumar, P.S.M.; Higuchi, K.; Yamamoto, Y.; Tokunaga, T.; Arai, S.; Ueda, S.; Hashimoto, A.; et al. Topologically immobilized catalysis centre for long-term stable carbon dioxide reforming of methane. *Chem. Sci.* **2019**, *10*, 3701–3705. [CrossRef] [PubMed]
11. Imai, T.; Ueda, S.; Nagao, S.; Hirata, H.; Deepthi, K.R.; Abe, H. N_2O-emission-free exhaust remediation by $Rh-NbO_x$ nanocomposites developed from Rh_3Nb alloy precursor. *RSC Adv.* **2017**, *7*, 9628–9631. [CrossRef]
12. Tanabe, T.; Imai, T.; Tokunaga, T.; Arai, S.; Yamamoto, Y.; Ueda, S.; Ramesh, G.V.; Nagao, S.; Hirata, H.; Matsumoto, S.; et al. Nanophase-separated Ni_3Nb as an automobile exhaust catalyst. *Chem. Sci.* **2017**, *8*, 3374–3378. [CrossRef] [PubMed]
13. Fujita, T.; Peng, X.; Yamaguchi, A.; Cho, Y.; Zhang, Y.; Higuchi, K.; Yamamoto, Y.; Tokunaga, T.; Arai, S.; Miyauchi, M.; et al. Nanoporous nickel composite catalyst for the dry reforming of methane. *ACS Omega* **2018**, *3*, 16651–16657. [CrossRef] [PubMed]
14. Fujita, T.; Abe, H.; Tanabe, T.; Ito, Y.; Tokunaga, T.; Arai, S.; Yamamoto, Y.; Hirata, A.; Chen, M.W. Earth-abundant and durable nanoporous catalyst for exhaust-gas conversion. *Adv. Funct. Mater.* **2016**, *26*, 1609–1616. [CrossRef]
15. Huang, J.; Yang, B.; Chen, H.; Wang, H. Thermodynamic optimisation of the Ni-Al-Y ternary system. *J. Phase Equilib. Diffus.* **2015**, *36*, 357–365. [CrossRef]
16. Li, Q.; Feng, C.; Jiao, Q.; Guo, L.; Liu, C.; Xu, H.B. Shape-controlled synthesis of yttria nanocrystals under hydrothermal conditions. *Phys. Stat. Sol. (a)* **2004**, *201*, 3055–3059. [CrossRef]